第33卷 第8期 焊 接 学 报 Vol. 33 No. 8
2012年8月 TRANSACTIONS OF THE CHINA WELDING INSTITUTION August 2012

基于 FEM 的高速列车地板结构焊接顺序优化

王 苹，王 强，刘雪松，方洪渊
(哈尔滨工业大学 先进焊接与连接国家重点实验室，哈尔滨 150001)

摘 要： 借助非线性有限元软件 MSC. Marc，模拟了高速列车铝合金挤压型材地板结构在现行工艺条件下的焊接变形. 为提高计算精度，采用移动的双椭球热源模型模拟 MIG 焊接过程，母材 6N01 和焊丝 ER5356 两种材料随温度变化的热物理性能参量. 结果表明，采用 7 块铝合金挤压型材拼焊的高速列车地板结构，焊后地板结构在各焊缝位置上沿厚度方向上(y 向) 产生正 V 形的角变形，地板结构纵向中心横截面上最大挠曲变形为 14.86 mm. 在此工作基础上提出由外侧向中心侧对称焊接地板结构的优化方案，焊后变形规律与现行工艺一致，但是横向挠曲变形量仅为现行工艺条件下的 78.6%. 对于大型复杂构件，可以利用结构自身重力的作用控制焊接变形.

关键词： 高速列车地板；铝合金挤压型材；控制变形；焊接顺序
中图分类号： TG404 **文献标识码：** A **文章编号：** 0253－360X(2012)08－0045－04

王 苹

0 序 言

大型 Al-Mg-Si 系铝合金挤压型材合金 6N01 因其薄壁、中空、加工及可焊性能好、型材长度可达 25～30 m(与车体同长)，被广泛应用于新型高速列车车体的地板、侧墙和顶棚等部位[1,2]. 采用铝合金挤压型材使得车辆的制造工序大为缩减，生产中采用 MIG 焊，实现自动化生产的同时大大提高了生产效率[3]. 高速列车地板结构虽不是主要的承载部位，但是对焊接变形的控制很严格，尤其是平面度的控制要求很高. 地板结构正反两面各有长度为 25 m 的 6 条纵向焊缝，若采用试验方法进行焊接变形规律或变形控制，周期长、成本高，并且还需要掌握各个因素影响焊接变形的内在规律.

基于计算机技术和专业知识的计算机辅助技术(CAE)，特别是数值模拟技术的有限单元法(FEM)以其高效率、低成本的强烈优势在材料加工领域，尤其是大型复杂结构件的热加工成形研究中得到了广泛的应用[4－8]. 因此文中借助于非线性有限元软件 MSC. Marc，对高速列车地板结构焊接过程进行数值模拟，量化了不同焊接顺序下的焊接变形，并进行了理论分析，以此为工艺完善及工程应用提供数据支撑.

收稿日期：2012－03－12
基金项目：中俄政府间科技合作资助项目(2007DFR0070)

1 有限元模型建立

1.1 网格划分

高速列车地板结构是由 7 块长度为 25 m，宽度为 432 mm 的铝合金挤压型材焊接而成，地板焊接结构局部的几何尺寸见图 1.

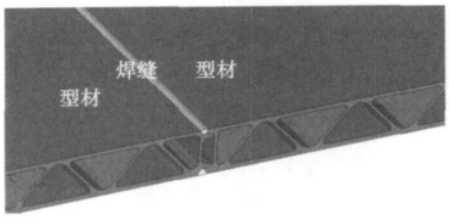

图 1 地板局部的几何模型
Fig. 1 Local view of geometrical rail floor

几何模型的地板长度为 1 200 mm，网格模型为三维实体模型，网格最小尺寸为 5 mm × 4 mm × 3 mm，采取疏密过渡方法划分网格来提高计算效率. 模型单元为八节点六面体，采用全积分单元计算，地板结构模型中共 102 700 个单元，181 216 个节点，见图 2. 分析软件为 MSC. Marc 2005，计算平台为曙光工作站.

1.2 材料特性参数

材料的热物理性能参数对模拟结果的精度影响很大. 焊接过程是一个涉及到金属先加热后冷却的

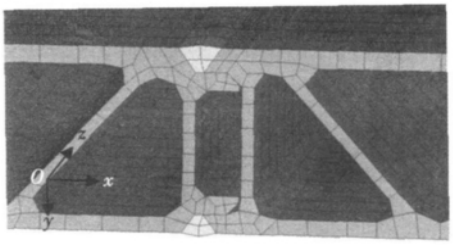

图 2 地板结构有限元模型

Fig. 2 FEM model of rail floor

过程，因此需要考虑 6N01 铝合金和焊丝 ER5356 动态的热物理性能参数，见图 3. 母材 6N01 和焊丝 ER5356 均设定为各向同性，泊松比为 0.283，质量密度为 2 730 kg/m^3，质量密度为重力作用的输入参数.

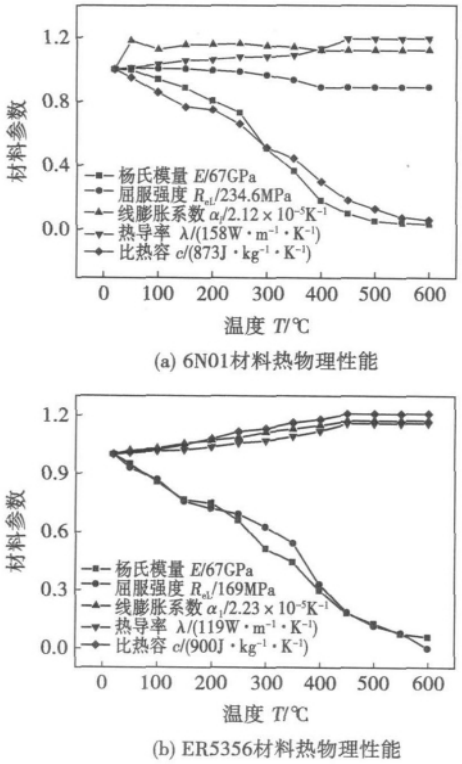

(a) 6N01材料热物理性能

(b) ER5356材料热物理性能

图 3 6N01 和 ER5356 的材料参数

Fig. 3 Material properties of 6N01 and ER5356

2 焊接工艺参数

2.1 焊接顺序

7 块铝合金挤压型材组对点固之后施焊，地板结构正面共有 6 条纵向焊缝的分布见图 4. 焊接夹具仅在施焊之初对组对地板施加 x 向挤压力，焊接过程中不考虑夹具作用.

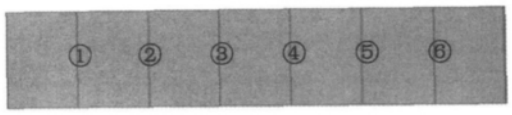

图 4 焊缝位置示意图

Fig. 4 Sketch map of welding seam

基于现行工艺条件下的焊接顺序方案，并结合生产环节中的可操作性，文中又提出了两种优化方案，3 种方案的焊接顺序见表 1.

表 1 焊接顺序方案

Table 1 Schemes of welding sequence

方案	焊接顺序
现行工艺	(①+④)→(②+⑤)→(③+⑥)
优化方案 1	(③+④)→(②+⑤)→(①+⑥)
优化方案 2	(①+⑥)→(②+⑤)→(③+④)

2.2 焊接工艺参数

采用 99.999% 氩气保护，气体流量为 40 L/min，焊接工艺参数见表 2. 现有的焊接热源模型中，文中采用移动的双椭球热源模型来模拟 MIG 焊.

表 2 焊接工艺参数

Table 2 Welding process parameters

焊丝直径 d/mm	焊接电流 I/A	电弧电压 U/V	焊接速度 v/(cm·min^{-1})	热输入 Q/(J·cm^{-1})
1.2	205～215	21～23	70～75	3 973

3 试验结果与讨论

3.1 模拟角变形结果

模拟中仅考虑了正面 6 条纵向长焊缝，MIG 焊时需要添加熔融状态的焊丝，近缝区金属由于热作用会产生压缩塑性应变，焊后冷却时又会受到拉伸作用. 冷却至室温时，焊缝附近的塑性变形沿着型材厚度方向上的不协调导致横向角变形，各角变形的积累将使焊后地板结构会产生明显的横向的挠曲变形，6 条焊缝产生的角变形累加的效果如图 5 所示，这使得地板的平面度受到很大影响.

由于挤压型材特殊的中空结构形式，模拟结果表明焊后在纵向(型材的挤压方向)未出现挠曲变形. 提取地板长度方向中心横截面上的焊后变形结果见图 6. 3 种工艺方案下的焊后变形趋势相同，均表现为地板结构沿着厚度方向(y 向)呈现正 V 字形的角变形，由于角变形而引起的地板结构的最大

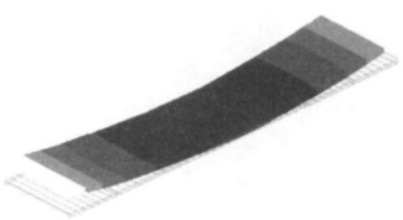

图 5　焊后地板变形示意图

Fig. 5　Deflection of welded rail floor assembly

横向挠曲变形量在现行工艺、优化方案 1 和优化方案 2 这 3 种工艺下依次为 14.86,15.38,11.68 mm. 对比发现,现行工艺和优化方案 1 的变形差别不大,而优化方案 2,也就是对 7 块型材由外侧向中心的对称焊接顺序控制焊后变形的效果明显,为现行工艺下变形量的 78.6%.

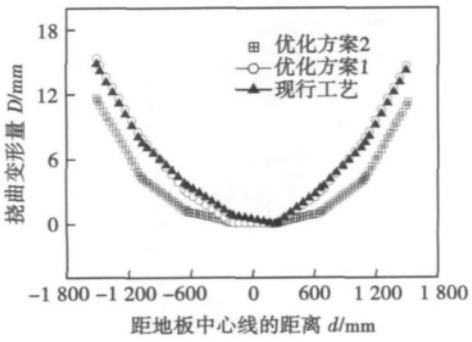

图 6　3 种方案下的地板结构的焊后挠曲变形

Fig. 6　Deformation of welded rail floor for three schemes

采用 3 种焊接方案的高速列车地板结构各焊缝的焊后角变形值参见表 3. 优化方案中均采用对称的焊接顺序,因此同时焊接的两条焊缝,焊缝③和焊缝④、焊缝②和焊缝⑤以及焊缝①和焊缝⑥的焊后角变形基本相同,焊后地板结构的变形也是对称的,而在现行工艺的焊接顺序下,焊后地板结构的各角焊缝焊后角变形差异明显.

表 3　3 种焊接顺序下各焊缝的角变形(°)

Table 3　Angular distortion of each weld seam for three welding schemes

焊缝	现有工艺	优化方案 1	优化方案 2
①	179.604	179.736	179.499
②	179.832	179.696	179.704
③	179.755	179.634	179.866
④	179.438	179.595	179.858
⑤	179.873	179.693	179.714
⑥	179.640	179.737	179.483

进一步比较两种优化方案下地板结构的焊后角变形结果,发现优化方案 1 中焊接顺序是由中心向外侧对称焊接,焊后由内侧的焊缝③和焊缝④向外侧的焊缝①和焊缝⑥角变形逐渐变小; 优化方案 2,焊接顺序是由外侧向中心对称焊接,外侧的焊缝①和焊缝⑥焊后角变形最大,内侧的焊缝③和焊缝④角变形很小,接近 180°.

分析造成这种变形规律原因是在焊接过程中,地板结构的自身重力对角变形的抑制作用造成的. 焊前对型材进行了点焊定位,其连接形式属于局部连接,点固的两块型材没有形成一个完全的刚性连接,结构的整体性较差. 当相邻的两块型材焊接时,与之点固连接的远端型材对施焊部位的角变形的作用较弱,反之,若远端型材已经焊接,由于整体的刚性大,其重力造成三点弯曲抑制正在施焊焊缝的角变形效果就会明显.

以优化方案 2 为例,由外侧向中心对称焊接 6 条纵向焊缝,当完成外侧焊缝①时,由焊缝连接的两块型材变为一个刚性体,其重力会对内侧焊缝②产生一个力矩的作用,产生横向拉应力延展焊缝,减小其压缩塑性变形量,使得焊缝②角变形变小,此后结构的刚性进一步加大,重力力矩作用也变大,进而使得最后施焊的焊缝③焊后角变形最小,接近于 180°. 结构自身重力作用同样适用于优化方案 1 中的角变形变化规律.

3.2　变形结果比较

在高速列车生产现场分别对 10 个完整的地板结构中 6 条焊缝的焊后变形采集数据,各焊缝自左向右的标号依次为 1 号,2 号,3 号,4 号,5 号,6 号. 将采集数据的平均值与 3 种焊接顺序方案中对应位置的有限元模拟计算结果绘制成曲线进行对比,见图 7.

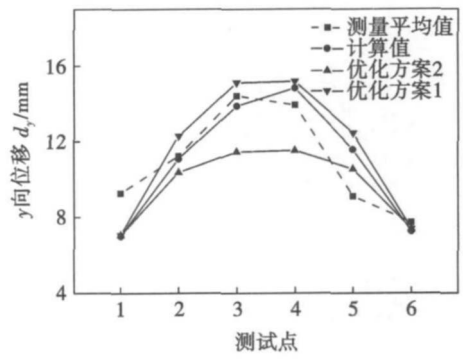

图 7　测试与模拟的变形曲线对比

Fig. 7　Curves of tested and simulated deformation

由于现行工艺条件的不稳定性,现场测试数据

的波动较大,但是测试的平均值基本上与模拟现行方案中的数据相吻合; 优化方案 1 的焊后变形量大于现行的工艺方案和测试值,这说明由中心向外侧对称焊接地板结构 6 条纵向焊缝的方案不可取; 优化方案 2 的变形量均小于现行工艺,因此采用此种焊接顺序来控制铝合金挤压型材地板结构的焊接变形是较为理想的,是易操作实施的方案.

4 结 论

(1) 现行工艺条件下,基于热 - 力耦合有限元理论,采用移动双椭球热源以及随温度变化的母材和焊丝的热物理性能参量,模拟 7 块铝合金挤压型材拼焊高速列车的地板结构,焊后地板结构各焊缝造成的角变形累加使地板结构产生横向挠曲变形,最大挠曲量为 14.86 mm,模拟结果与实测数据基本一致.

(2) 针对现有工艺,提出的由外侧向中心对称焊接地板结构上的 6 条纵焊缝的方案,焊后挠曲变形规律与现行工艺一致,但是变形量仅为现行工艺条件下的 78.6%.

(3) 对于类似地板结构的大型复杂薄壁构件,可以利用结构自身重力造成的三点弯曲作用,制定合理的工艺措施来控制焊接角变形,矫正其平面度偏差.

参考文献:

[1] 王元良, 洛德阳, 王一戎. 我国高速列车焊接技术及其新发展 [J]. 电焊机, 2008, 38(8): 8 - 12.
Wang Yuanliang, Luo Deyang, Wang Yirong. Welding and its development of bullet train [J]. Electric Welding Machine, 2008, 29(10): 45 - 49.

[2] 李瑞淳, 王 骏. 德国高速列车综述 [J]. 国外铁道车辆, 2005, 42(6): 1 - 6.
Li Ruichun, Wang Ai. Survey of high speed trains in Germany [J]. Foreign Rolling Stock, 2005, 42(6): 1 - 6.

[3] 杨尚磊, 孟立春, 吕任远, 等. 高速车辆用 A6N01 铝合金的脉冲 MIG 焊 [J]. 焊接, 2008(9): 33 - 35.
Yang Shanglei, Meng Lichun, Lü Renyuan, *et al*. Pulsed MIG welding of A6N01 Al alloy used in high speed vehicle [J]. Welding & Joining, 2008(9): 33 - 35.

[4] 焦立新. 焊接仿真技术应用与未来发展 [J]. 航空制造技术, 2008(8): 48 - 50.
Jiao Lixin. Application and future of welding simulation technology [J]. Aeronautical Manufacturing Technology, 2008(8): 48 - 50.

[5] 曾 志, 王立君. 数值模拟技术在焊接中的应用 [J]. 航空制造技术, 2008(8): 44 - 47.
Zeng Zhi, Wang Lijun. Application of numerical simulation technology in welding [J]. Aeronautical Manufacturing Technology, 2008(8): 44 - 47.

[6] 王中辉, 李冬雪. 焊接数值模拟技术的发展现状 [J]. 焊管, 2010, 33(6): 28 - 31.
Wang Zhonghui, Li Dongxue. Development status of welding numerical simulation technology [J]. Welded Pipe and Tube, 2010, 33(6): 28 - 31.

[7] 周广涛, 刘雪松, 闫德俊, 等. 顶板焊接顺序优化减小焊接变形的预测 [J]. 焊接学报, 2009, 30(9): 109 - 112.
Zhou Guangtao, Liu Xuesong, Yan Dejun, *et al*. Prediction for welding deformation reducing by welding sequence optimization of upper plate [J]. Transactions of the China Welding Institution, 2009, 30(9): 109 - 112.

[8] 杨建国, 陈绪辉, 张学秋. 高能束焊接数值模拟可变新型热源模型的建立 [J]. 焊接学报, 2010, 31(2): 24 - 27.
Yang Jianguo, Chen Xuhui, Zhang Xueqiu. Numerical modeling of new alterable heat source based on high energy welding beam [J]. Transactions of the China Welding Institution, 2010, 31(2): 24 - 27.

作者简介: 王 苹,女,1983 年出生,博士研究生. 主要从事焊接结构应力变形控制、数值模拟计算及可靠性评估研究. 发表论文 6 篇. Email: nancyhit2007@sina.com

通讯作者: 刘雪松,男,副教授. Email: liuxuesong@hit.edu.cn

Abstract: In order to improve the equal bending load-carrying capacity (EBLCC) of under-matched butt joints in the elastic stage, the shape design of the reinforcement was investigated based on materials mechanics under three-point bending load. The design idea, criterion and realization condition of EBLCC were put forward. Two design methods for the reinforcement shape were proposed after theoretical calculation of under-matched butt joints under three-point bending load. The theoretical analysis results were verified by the finite element method. The research results showed that the reinforcement shape from theoretical calculation was parabolic. The finite element results were basically coincident with the theoretical analysis. The vulnerable area of under-matched welded joints can be transferred from the weld bead to base metal near the weld toe after the shape design of the reinforcement of EBLCC, which improved the bending load-carrying and resistance to bending deformation capacity of under-matched butt joints. The arc shape can replace the parabolic shape for the double-side symmetric reinforcement. The proposed shape design method has potential application in the design of under-matched butt joints of high strength steels.

Key words: high strength steel; under-matched welded joints; equal bending load-carrying capacity; shape design of the reinforcement; finite element verification

Dual-channel signal acquisition and characteristics analysis of arc sound in pipe MIG welding LIU Lijun[1,2], ZHOU Bintao[1], DAI Hongbin[1], BI Shujuan[1,3], LAN Hu[1], ZHANG Huajun[1] (1. School of Material Science & Engineering, Harbin University of Science and Technology, Harbin 150080, China; 2. Ningbo Institute of Technology, Zhejiang University, Ningbo 315100, China; 3. School of Science, Harbin Institute, Harbin 150086, China). pp 41 – 44

Abstract: Dual-channel signal acquisition and characteristic analysis was investigated in pipe MIG welding. Since the echo interference is relatively large in the closed space within pipe, the two-channel arc sound signals were studied with the independent component analysis (ICA). The ICA signals were denoised with wavelet. The signal-to-noise ratio was obviously improved. The relationship between the arc sound signals inside and outside the pipe and weld penetration status was analyzed from time, frequency and time-frequency domain, respectively. The experimental results showed that the amplitude of signal energy was related to the weld penetration status. The signal energy increased with the increasing of weld penetration. The research in this paper provides technical basis for monitoring welding quality with arc signal.

Key words: pipe MIG welding; arc sound; independent component analysis; wavelet transform; penetration

Welding sequence optimization for high-speed rail floor based on FEM WANG Ping, WANG Qiang, LIU Xuesong, FANG Hongyuan (State Key Laboratory of Advanced Welding and Joining, Harbin Institute of Technology, Harbin 150001, China). pp 45 – 48

Abstract: Based on the thermo-mechanical coupling analysis with nonlinear commercial software MSC. Marc, the welding deformation of large-scale hollow extruded aluminum alloy high-speed rail floor was simulated under present technological conditions. A moving double-ellipsoid heat source was employed in the model for MIG welding process, and the dynamic mechanical and thermal-physical properties of the 6N01 aluminum alloy and ER5356 filler metal were adopted to improve the calculation precision. The results show that the as-welded deformation of rail floor joined by seven pieces of aluminum alloy extrusion profiles was V-type angular distortion in the thickness direction, and the maximum deflection was 14.86 mm in the horizontal direction. Moreover, an optimized welding sequence was put forward, which was symmetrically welding from the lateral to the center. With the same deformation tendency, the deflection of the optimized rail floor weld was reduced to 78.6% of that under the present scheme. For large-scale and complex structures, gravity should be seriously considered for control of welding deformation.

Key words: high-speed rail floor; extrusion profile of aluminum alloy; deformation control; welding sequence

Weldability of Zr-Ti microalloyed high-strength high-toughness structural steels LU Weiyu[1], WU Kaiming[1], WANG Honghong[1], LEI Xuanwei[1], YIN Yuqun[2], YAO Yongkuan[2], WANG Daoyuan[2] (1. International Research Institute for Steel Technology, Wuhan University of Science and Technology, Wuhan 430081, China; 2. Nanjing Iron & Steel Group Co., Ltd., Nanjing 210035, China). pp 49 – 52

Abstract: The continuous cooling transformation curves (SH-CCT) in the heat affected zone (HAZ) of F550 steel plate were established with thermal simulation, and the microstructural evolution and mechanical properties of the HAZ were investigated. Experimental results showed that fine Zr and Ti complex oxides dispersed in the steel weld, which have pinning effect on the austenite grain in the coarse-grained heataffected zone (CGHAZ) due to the combined deoxidation of Zr and Ti in the steel plate. Meanwhile, the low carbon content and proper addition of Ni, Cr, Cu and Mo were adopted in the design of high-strength steel. Consequently, the bainitic microstructure with small amount of dispersing M-A islands was obtained in the HAZ in a large range of heat input (25 – 100 kJ/cm). The results of V-notch impact test of CGHAZ welded by submerged arc welding with heat input of 50 kJ/cm indicated that the impact toughness of F550 steel was good at −60 ℃.

Key words: Zr-Ti microalloying; SH-CCT curve; weldability; low temperature impact toughness; submerged arc welding

Effect of processing parameters on microstructure and mechanical properties of Al_2O_3/TC4 alloy joints YANG Minxuan[1], LIN Tiesong[1,2], Han Chun[1], He Peng[1], Wei Hongmei[1] (1. State Key Laboratory of Advanced Welding and Joining, Harbin Institute of Technology, Harbin 150001, China; 2. School of Materials Science and Engineering, Harbin Institute of Technology, Harbin 150001, China). pp 53 – 56

Abstract: Al_2O_3 and TC4 alloy were brazed with Cu + B brazing filler at 890 – 970 ℃ for 10 min and at 930 ℃ for 0 – 30 min, respectively. The microstructure and mechanical properties of the resultant joints were investigated with SEM, EDS and shear testing machine. The results indicated that with the increasing of brazing temperature and holding time, the thickness of Ti4(Cu,Al)$_2$O layer increased, next to which continuous and thick Ti_2(Cu,Al) existed, and the amounts of Ti_2(Cu,Al) and Ti + Ti_2(Cu,Al) increased. The size and distribution range of Ti + Ti_2(Cu,Al) also increased, which migrated to the TC4 alloy side. The hypereutectoid regions widened near the TC4 alloy. Below 950 ℃, the TiB whiskers were mainly dispersed on Al-